

Bayberry tannin directed assembly of bifunctional graphene aerogel for simultaneously solar steam generation and uranium adsorption

Fangwu Wu,^{a,b#} Dan Liu,^{c,d#} Guangyong Li,^a Liqiang Li,^a Lifeng Yan,^e Guo Hong,^{*c,d}
and Xuetong Zhang^{*a,f}

^a Suzhou Institute of Nano-tech and Nano-bionics, Chinese Academy of Sciences, Suzhou, 215123, P.R. China

^b Nano Science and Technology Institute, University of Science and Technology of China, Suzhou, 215123, P.R. China

^c Institute of Applied Physics and Materials Engineering, University of Macau, Avenida da Universidade, Taipa, Macau SAR

^d Department of Physics and Chemistry, Faculty of Science and Technology, University of Macau, Avenida da Universidade, Taipa, Macau SAR 999078.

^e CAS Key Laboratory of Soft Matter Chemistry, iChEM, and Department of Chemical Physics, University of Science and Technology of China, Hefei 230026, China

^f Division of Surgery & Interventional Science, University College London, London NW3 2PF, United Kingdom

#Contributed equally

1. Property of bayberry tannin

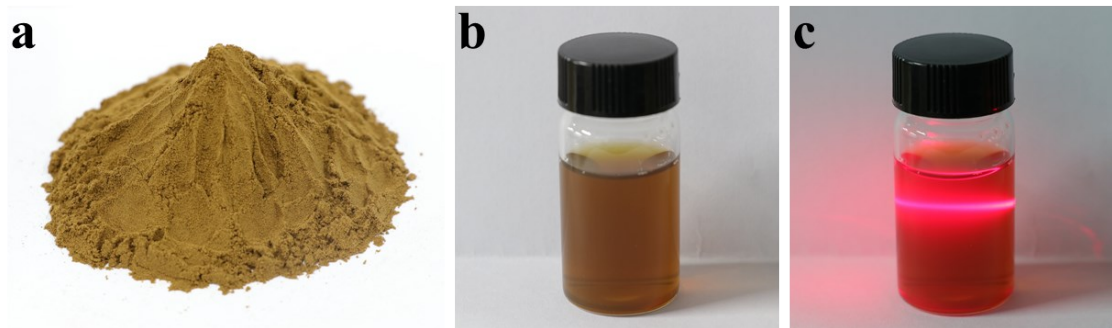


Figure S1. (a) Photo images of BT powder (b) BT dispersion in water (c) Tyndall effect of BT dispersion.

2. Photo images and dynamic shear rheology behavior of the BGA gel precursor and GO

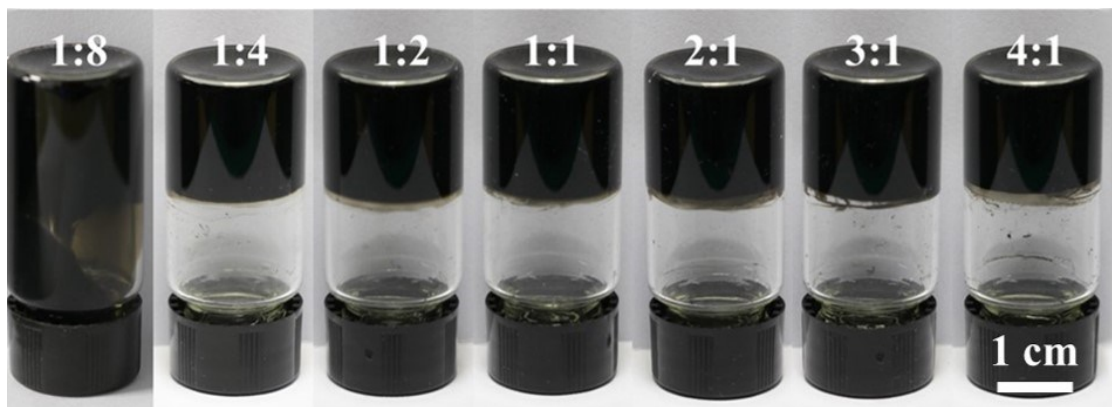


Figure S2. Photo images of the BGA gel precursors fabricated with BT to GO feeding mass ratio of 1/8, 1/4, 1/2, 1, 2, 3, and 4 (the concentration of GO is fixed at 8 mg/ml).

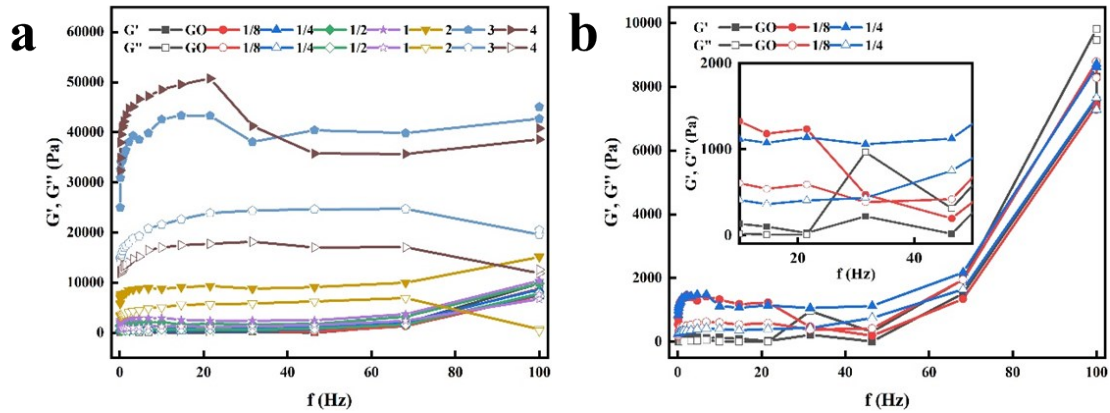


Figure S3. The curves of storage modulus (G') and loss modulus (G'') with frequency.

(a) BGA gel precursor prepared with different BT to GO feeding mass ratio and pure GO. (b) BGA gel precursor prepared with BT to GO feeding mass ratio of 1/8, 1/4, and pure GO.

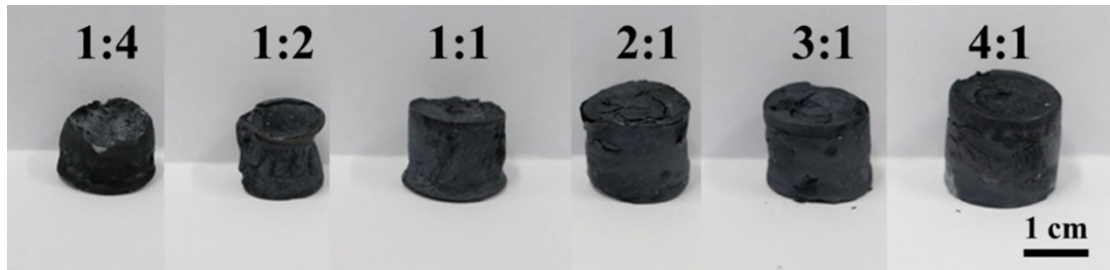


Figure S4. Photo images of the BGA fabricated with BT to GO feeding mass ratio of 1/4, 1/2, 1, 2, 3 and 4.

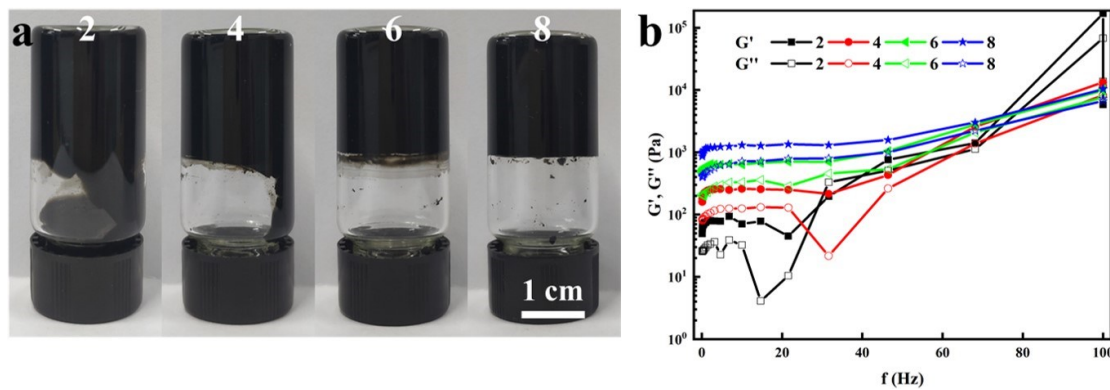


Figure S5. (a) Photo images of the BGA gel precursors fabricated with different GO concentration when the concentration of BT is fixed at 40 mg/ml. (b) The curves of storage modulus (G') and loss modulus (G'') with frequency for BGA gel precursors fabricated with different GO concentration.

3. Effect of pH on the sol-gel process

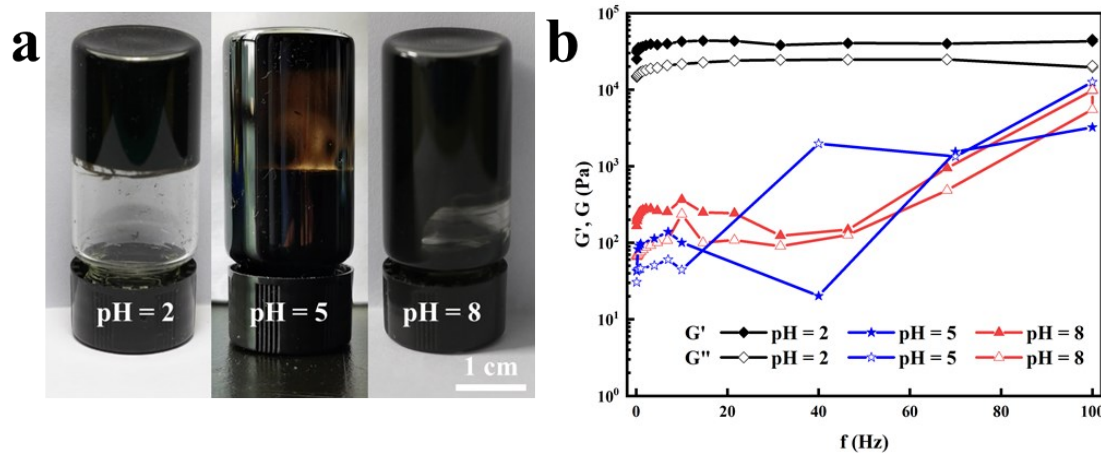


Figure S6. (a) Photo images of BGA gel precursor prepared at different pH. (b) The curves of storage modulus (G') and loss modulus (G'') with frequency for BGA gel precursor prepared at different pH.

4. Microstructure of the BGA

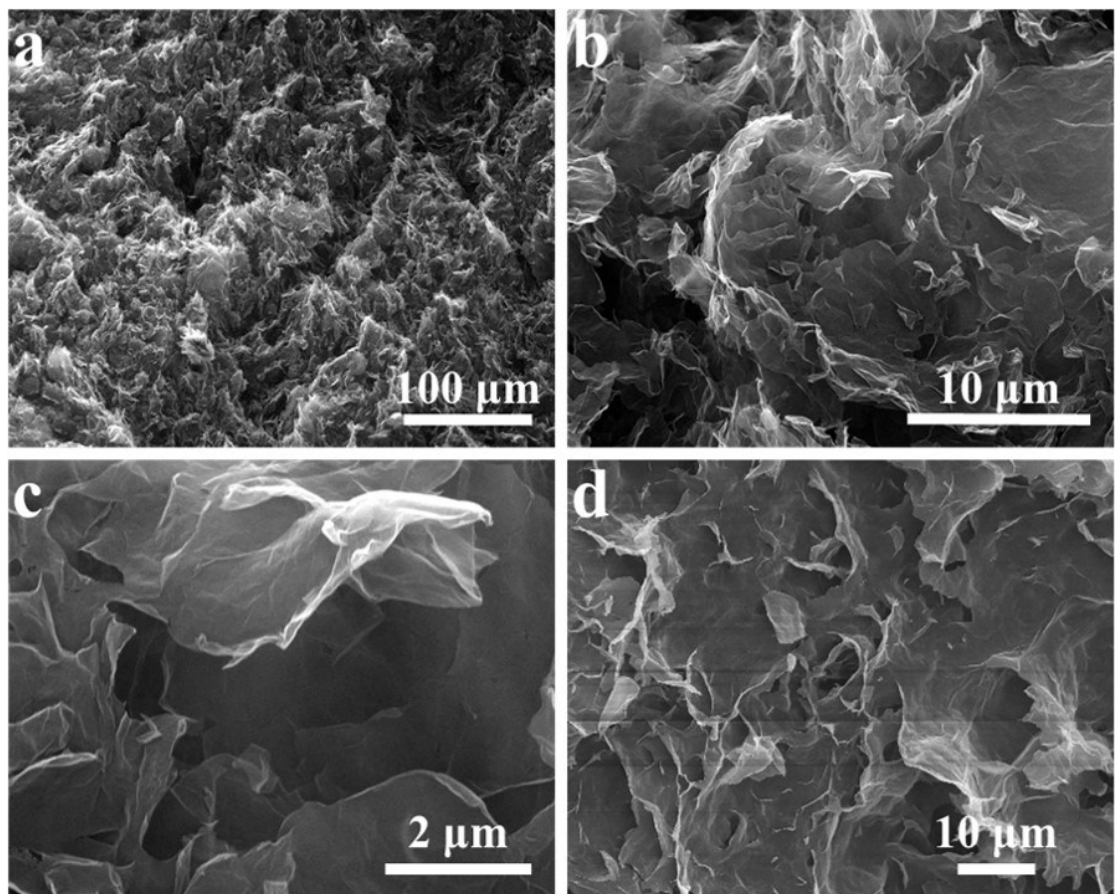


Figure S7. SEM image of BGA(a, b) and U-BGA(c, d).

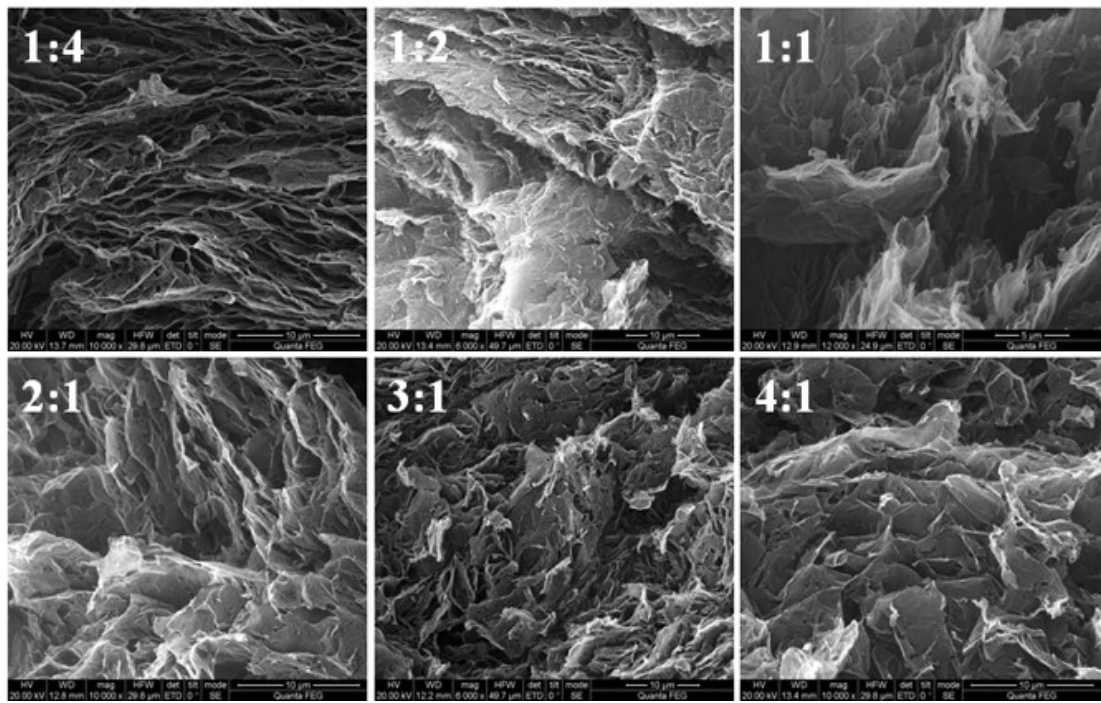


Figure S8. SEM images of BGA fabricated with different ratios.

5. Surface area and pore size distribution of BGA

Table S1. Statistics of BET surface area and pore volume of graphene aerogel reported over five years.

Materials	Drying Method	BET Surface Area (m ² /g)	Pore Volume (cm ³ /g)	Ref.
GA (ascorbic acid)	SC-CO ₂ drying	512	2.48	[1]
GA (hydrothermal method)	SC-CO ₂ drying	394	1.46	[2]
GA (H ₂)	SC-CO ₂ drying	867	1.90	[3]
AN-GA (HI)	SC-CO ₂ drying	379.1	1.065	[4]
GA (organic cross-linker)	SC-CO ₂ drying	584	2.96	[5]
GA (L-phenylalanine)	Freeze drying	117	0.991	[6]
NDGA (ethylenediamine)	Natural drying	190	0.6	[7]

This work (3:1)	SC-CO ₂ drying	310.27	0.72
-----------------	---------------------------	--------	------

Table S2. The analysis of the porous structure in BGA fabricated with BT to GO feeding mass ratio of 1/4, 1/2, 1, 2, 3 and 4.

feed ratio	BET Surface Area (m ² /g)	Pore Volume (cm ³ /g)	Average Pore Size (nm)
1/4	443.05	1.25	10.22
1/2	323.02	0.85	11.53
1	399.08	1.33	11.40
2	379.26	1.15	12.16
3	310.27	0.72	10.20
4	282.98	0.60	10.47
Freeze drying	236.85	0.89	15.45

6. The reduction mechanism of GO by BT

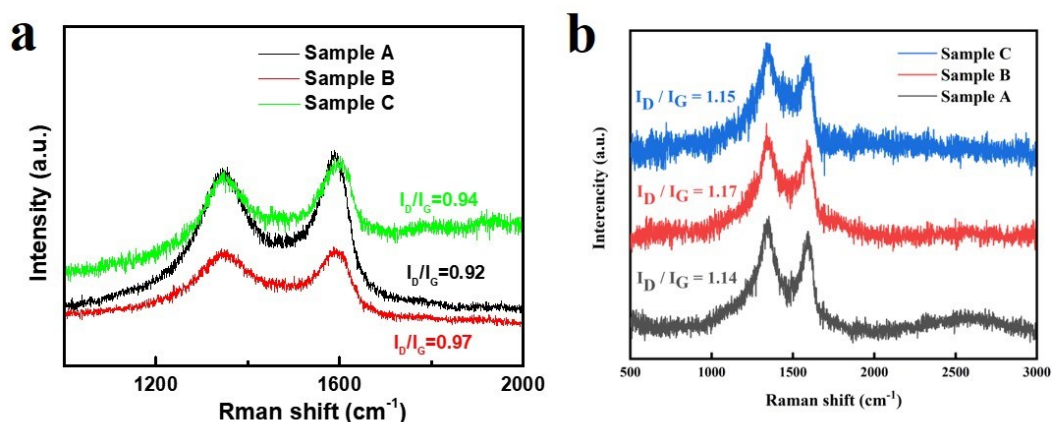


Figure S9. Raman spectra of GO (a) and BGA (b).

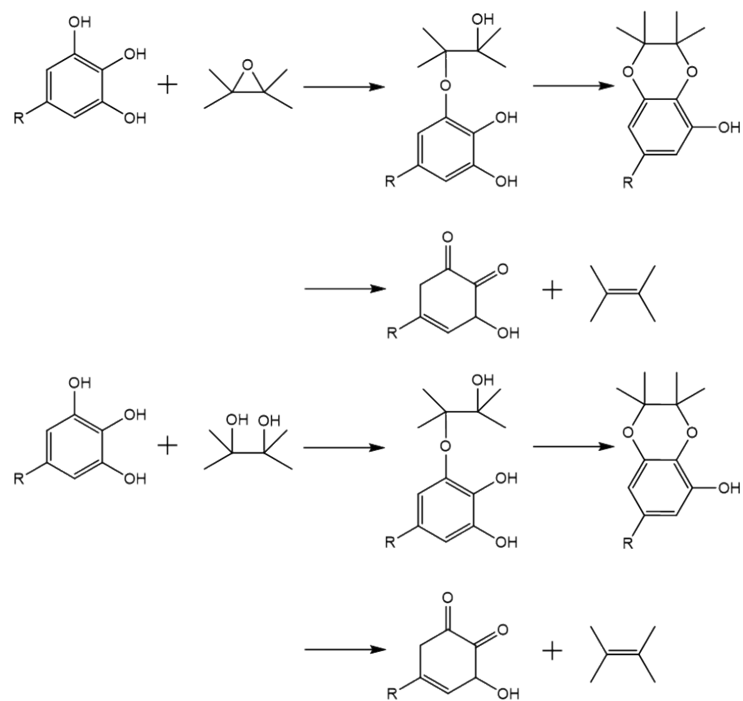


Figure S10. Possible mechanism for reduction of GO by BT.

7. IR spectra of BGA

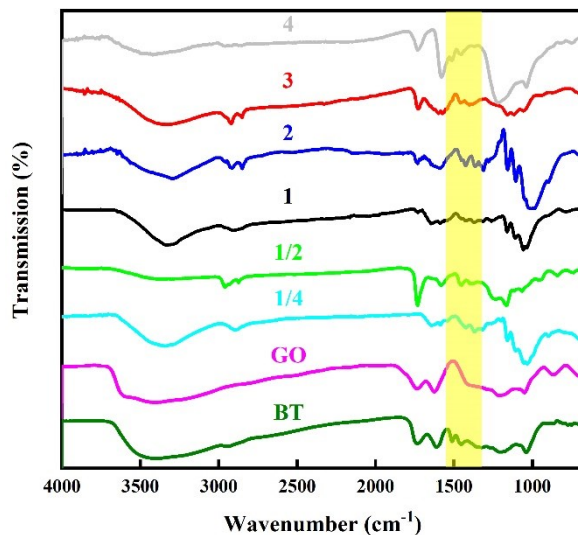


Figure S11. IR spectra of GO, BT and the BGA fabricated with BT to GO feeding mass ratio of 1/4, 1/2, 1, 2, 3 and 4.

8. Prussian blue method to confirm the BT in BGA

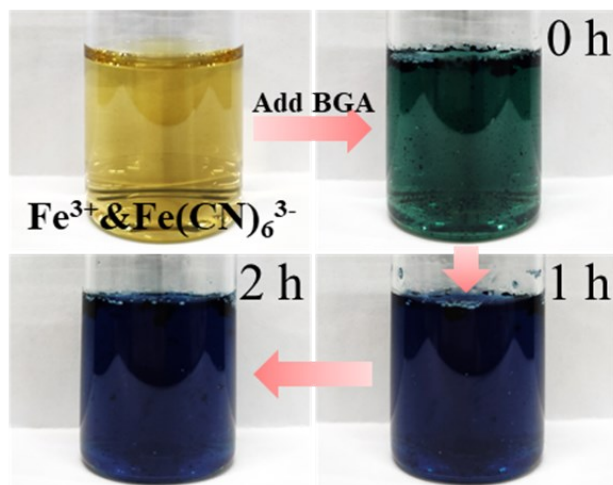


Figure S12. Photo images of the solution containing Fe^{3+} and $\text{Fe}(\text{CN})_6^{3-}$ after adding the BGA.

9. Comparison of water transport rate

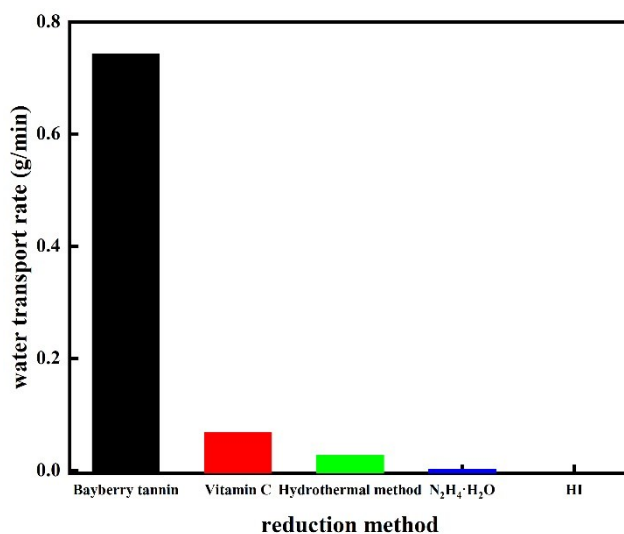


Figure S13. water transport rate of graphene aerogels reduced by bayberry tannin, vitamin C, hydrothermal method, hydrazine hydrate and hydroiodic acid, respectively.

10. Solar-thermal property of BGA

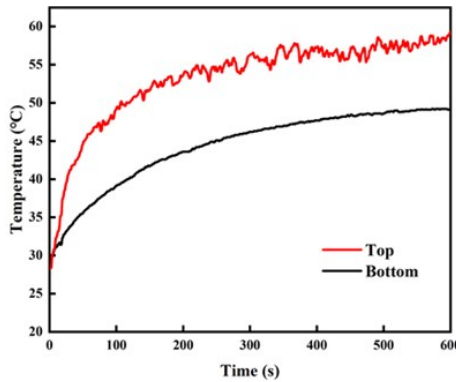


Figure S14. Temperature–time curves of top and bottom of the BGA under 1 sun illumination.

Table S3. Solar steam generation performance of different materials.

Materials	Water evaporation rate [kg/(m ² ·h)]	Conversion efficiency (%)	Ref.
RGO-SA-CNT aerogel	1.622	83	[8]
NGCA-600	1.558	90	[9]
srGA	1.78	91	[10]
RGO/MoS ₂ aerogel bead	0.90	62.1	[11]
PNGA	1.3542	93.8	[12]
RGO-SA-cellulose aerogel	2.25	88.9	[13]
h-G foam	1.4	93.4	[14]
3DG	2.6	87	[15]
PFS@rGO	1.375	88.8	[16]
BHMG	1.476	92.9	[17]
rGO foam	2.40	~100	[18]
rGO/PU	0.9	65	[19]
PAAm aerogel	2.0	85.7	[20]
Poly(vinyl alcohol) hydrogel	2.6	91%	[21]
Nanocellulose	1.13	78%	[22]
Aluminium nanoparticles	1.0	90%	[23]
Polymer foam	1.20	80%	[24]
Wood	1.08	74%	[25]
BGA	1.84	95.5	This work

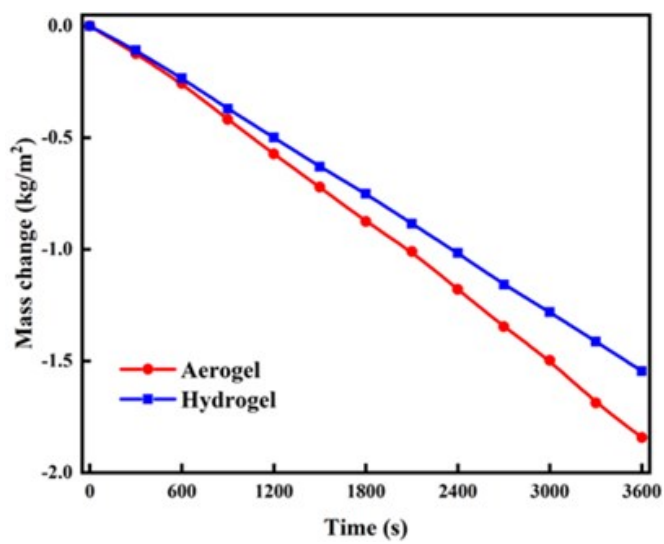


Figure S15. Water evaporation rate of the BGA and BGA gel precursor.

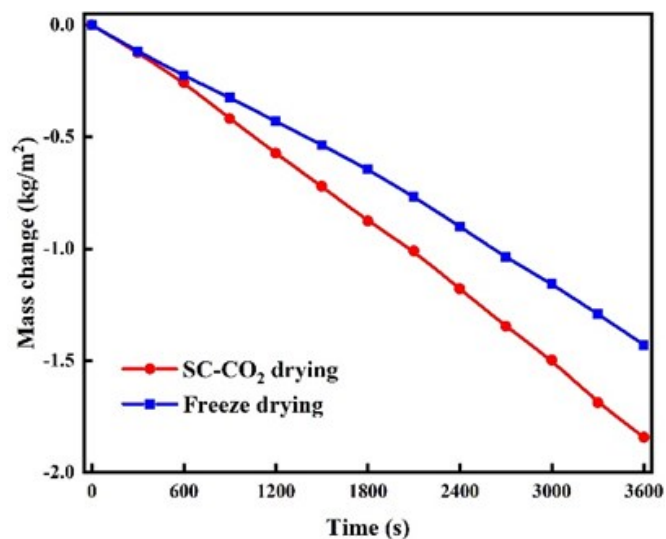


Figure S16. Water evaporation rate of the BGA fabricated with SC-CO₂ and Freeze drying.

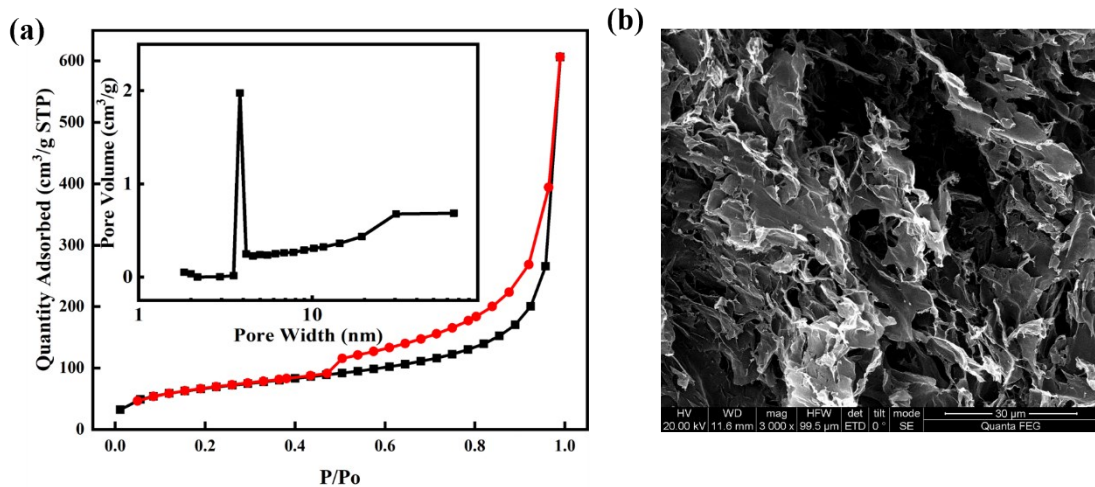


Figure S17. (a) Nitrogen adsorption and desorption isotherms, and pore size distribution of the BGA fabricated by freeze drying. (b) SEM image of the BGA fabricated with freeze drying.

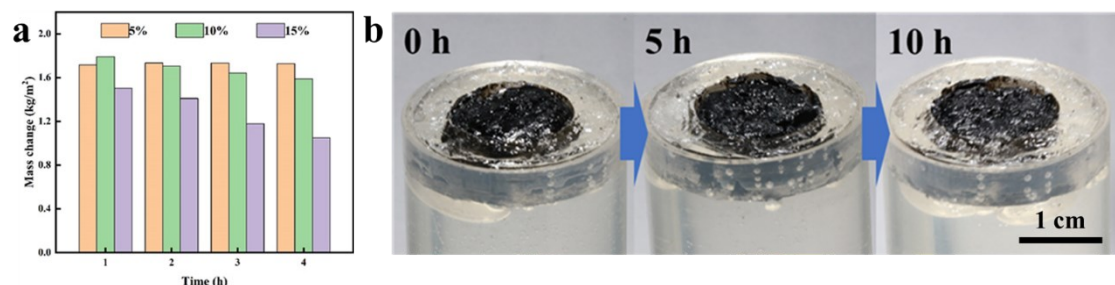


Figure S18 (a) Water evaporation rate of the BGA in salty water with different salinity from 5% to 15% (weight ratio). (b) Photo images of upper surface of the BGA when the light duration is 0 h, 5 h, 10 h.

The Calculation of the actual efficiency

According to reported method, the actual efficiency of BGA is calculated as follows:

$$\eta = \frac{\dot{m}(h_v + c \int_{T_0}^T dT)}{P_0} \quad (1)$$

c is the specific heat capacity of the water [kJ/(kg·°C)], T_0 and T is the initial and the final temperature of the system (°C).

It can be seen from Figure 3d that the starting temperature is 25 °C, and the ending temperatures of the upper and lower surfaces after 1 hour are 50 and 33 °C respectively. For the convenience of calculation, it is assumed that the temperature of BGA presents a trapezoidal distribution (the specific heat capacity of water is 4.2 kJ/(kg·°C)

Thus, $\eta=0.994$.

11. Uranium extraction performance of BGA

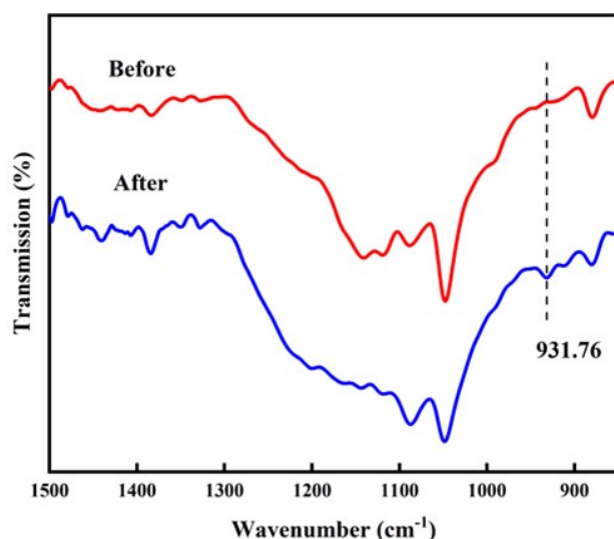


Figure S19. IR spectra of the BGA before and after uranium adsorption.

Table S4. Uranium extraction performance of graphene-based and other typical materials.

Materials	pH	Temp. (K)	Uranium adsorption (mg/g)	Ref.
GO-CS aerogel	8.3	RT	384.6	[26]
Fe-PANI-GA	5.5	298	350.47	[27]
FH/GOA	5.0	293	288.42	[28]
CA-PO4	5.5	298	150.3	[29]
phos-GOF	5~7	298	~483	[30]
GCZ8A	8.0	298.15	361.01	[31]
COF	6.0	298	408	[32]
PAF-NH(CH ₂) ₂ AO	6.0	298	385	[33]
MOF	9.0	298	118	[34]
Amidoxime-functionalized PAF	6.0	298	300	[35]
Polyamidoxime/polyethyleneimine magnetic graphene oxide	6.0	298	200	[36]
Hybrid MS@PIDO/Alg sponge	6.5	298	291.5	[37]
Porous aromatic framework	1.0	298	16	[38]
Amidoxime-functionalized wool fiber	8.0	298	80	[39]
Chimeric spidroin-based super uranyl-binding protein	7.0	298	12.3	[40]
BGA	5.0	298	279.10	This work

Table S5. The rates of uranium absorption of different materials.

Rate of uranium absorption (mg.g⁻¹.h⁻¹)	Materials	Reference
4.0	Cross-linked chitosan	[41]
0.4	MOF	[42]
16.7	MOF	[43]
13.3	PAF-1-NH(CH ₂) ₂ AO	[33]
15	MOF	[34]
25	amidoxime-functionalized PAF-1	[35]
20	polyamidoxime/ polyethyleneimine magnetic graphene oxide	[36]
12.6	hybrid MS@PIDO/Alg sponge	[37]
3	porous aromatic framework	[44]
0.8	porous aromatic framework	[38]
20.8	BP-PAO fiber	[45]
5.4	nano-ZnO loaded amidoxime- functionalized wool fiber	[39]
27.2	porous amidoxime-based nanofiber	[46]
40.8	amidoximated poly(imide dioxime) nanofiber	[47]
21.3	chimeric spidroin-based super uranyl- binding protein	[48]
31.25	BGA	This work

The Fitting of adsorption kinetics of BGA

According to adsorption kinetics, there are two kinds of kinetic models used to describe the adsorption behavior of UO₂²⁺, which are pseudo-first-order (2) and pseudo-second-order (3) kinetic models, respectively. The corresponding equations are listed as follows:

$$\ln(q_e - q_t) = \ln q_e - k_1 t \quad (2)$$

$$\frac{t}{q_t} = \frac{1}{k_2 q_e^2} + \frac{t}{q_e} \quad (3)$$

where q_e and q_t (mg/g) refer to the adsorption capacity at equilibrium and t time, respectively; k_1 (1/min) and k_2 [g/(mg·min)] are the rate constants of pseudo-first-order and pseudo-second-order kinetic models, respectively.

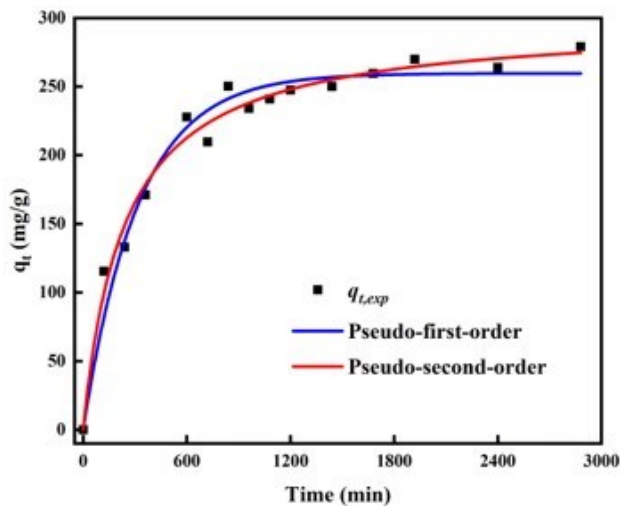


Figure S20. Uranium adsorption kinetics of BGA at 298 K (initial uranium concentration: 0.25 mg/mL, pH 5.0, V/m ratio: 2000 mL/g).

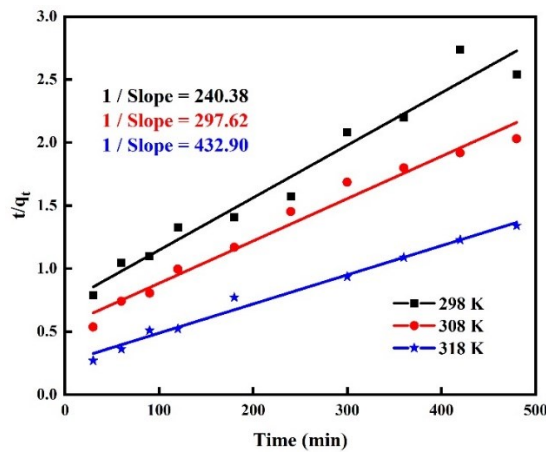


Figure S21. Uranium adsorption kinetics of BGA at different temperatures (initial uranium concentration: 0.025-0.25 mg/mL, pH 5.0, V/m ratio: 2000 mL/g). Regression by the pseudo-second-order equation.

Table S6. Fitting parameters of the pseudo-first-order and pseudo-second-order models

Temperature (K)	pseudo-first-order	pseudo-second-order
	R ²	R ²
298	0.91667	0.95961
308	0.94521	0.9755

The Fitting of adsorption isotherms of BGA

Both Langmuir and Freundlich models are used to fitting the experimental data. The equations are listed as follows:

$$\frac{c_e}{q_e} = \frac{c_e}{q_m} + \frac{1}{bq_m} \quad (1) \quad \text{Langmuir linear model}$$

$$\ln q_e = \ln k_F - \frac{1}{n} c_e \quad (2) \quad \text{Freundlich linear model}$$

where q_e and q_m (mg/g) are the equilibrium and maximum adsorption capacity, respectively; c_e (mg/mL) is the equilibrium concentration; b (mL/mg) is the Langmuir constant; k_F [(mg/g)×(mg/mL)^{-1/n}] is the Freundlich constant; n is an empirical parameter related to adsorption intensity.

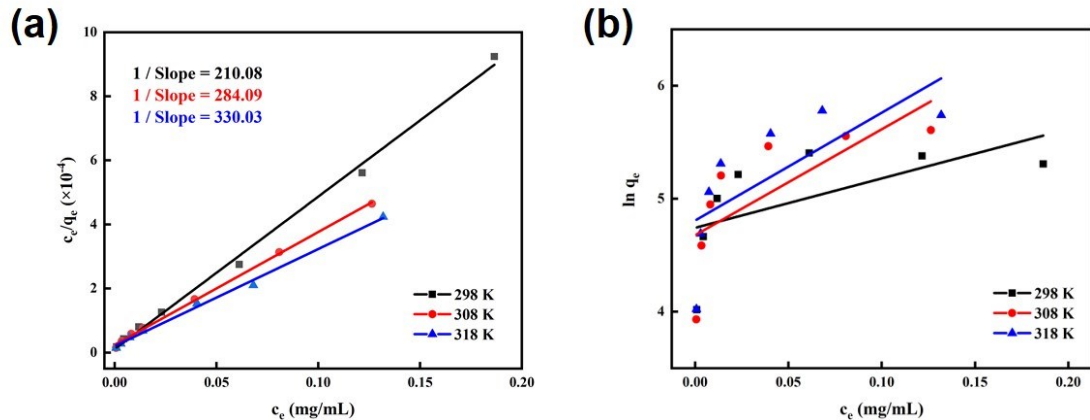


Figure S22. Uranium adsorption isotherms of BGA at different temperatures (initial uranium concentration: 0.25 mg/mL, pH 5.0, V/m ratio: 2000 mL/g). Regression by the Langmuir model (a) and Freundlich model (b).

Table S7. Fitting parameters of the Langmuir and Freundlich models

Temperature (K)	Langmuir			Freundlich
	R^2	$q_{m,cal}$ (mg/g)	$q_{m,exp}$ (mg/g)	R^2
298	0.99636	210.08	211.07	0.37646
308	0.99856	284.09	-	0.53865
318	0.99598	330.03	-	0.51788

Table S8. Uranyl ion and coexisting ion concentration before and after adsorption

Element (K)	Concentration ($\mu\text{g/L}$)	
	Before	After
U	18.6	8.6
Fe	50760	47460
Ni	1455.4	1334.8
Cu	1149.2	882.4
Zn	2830	2268
Pb	201.4	167.4
Na	11.44×10^6	11.38×10^6
Mg	1.37×10^6	1.32×10^6
Ca	0.49×10^6	0.46×10^6

Reference

- [1] X. T. Zhang, Z. Y. Sui, B. Xu, S. F. Yue, Y. J. Luo, W. C. Zhan, B. Liu, *J. Mater. Chem.* **2011**, 21, 6494.
- [2] S. T. Nguyen, H. T. Nguyen, A. Rinaldi, N. P. V. Nguyen, Z. Fan, H. M. Duong, *Colloid. Surface. A* **2012**, 414, 352.
- [3] X. Z. Wu, J. Zhou, W. Xing, G. Q. Wang, H. Y. Cui, S. P. Zhuo, Q. Z. Xue, Z. F. Yan, S. Z. Qiao, *J. Mater. Chem.* **2012**, 22, 23186.
- [4] G. Y. Li, X. T. Zhang, J. Wang, J. H. Fang, *J. Mater. Chem.* **2016**, 4, 17042.
- [5] M. A. Worsley, P. J. Pauzauskie, T. Y. Olson, J. Biener, J. H. Satcher, T. F. Baumann, *J. Am. Chem. Soc.* **2010**, 132, 14067.
- [6] L. M. Xu, G. Y. Xiao, C. B. Chen, R. Li, Y. Y. Mai, G. M. Sun, D. Y. Yan, *J. Mater. Chem. A* **2015**, 3, 7498.
- [7] X. Xu, Q. Q. Zhang, Y. K. Yu, W. L. Chen, H. Hu, H. Li, *Adv. Mater.* **2016**, 28, 9223.
- [8] X. Hu, W. Xu, L. Zhou, Y. Tan, Y. Wang, S. Zhu, J. Zhu, *Adv. Mater.* **2017**, 29, 1604031.
- [9] B. B. Huo, D. G. Jiang, X. Y. Cao, H. Liang, Z. Liu, C. W. Li, J. Q. Liu, *Carbon* **2019**, 142, 13.
- [10] P. P. Zhang, Q. H. Liao, T. Zhang, H. H. Cheng, Y. X. Huang, C. Yang, C. Li, L. Jiang, L. T. Qu, *Nano Energy* **2018**, 46, 415.
- [11] X. M. Feng, J. L. Zhao, D. W. Sun, L. Shanmugam, J. K. Kim, J. L. Yang, *J. Mater. Chem. A* **2019**, 7, 4400.
- [12] Z. Zhang, P. Mu, J. X. Han, J. X. He, Z. Q. Zhu, H. X. Sun, W. D. Liang, A. Li, *J.*

Mater. Chem. A **2019**, 7, 18092.

- [13] D. P. Storer, J. L. Phelps, X. Wu, G. Owens, N. I. Khan, H. L. Xu, *ACS Appl. Mater. Inter.* **2020**, 12, 15279.
- [14] H. Ren, M. Tang, B. Guan, K. Wang, J. Yang, F. Wang, M. Wang, J. Shan, Z. Chen, D. Wei, *Adv. Mater.* **2017**, 29, 1702590.
- [15] Y. Yang, R. Q. Zhao, T. F. Zhang, K. Zhao, P. S. Xiao, Y. F. Ma, P. M. Ajayan, G. Q. Shi, Y. S. Chen, *ACS Nano* **2018**, 12, 829.
- [16] T. J. Chen, S. Wang, Z. Z. Wu, X. D. Wang, J. Peng, B. H. Wu, J. Q. Cui, X. L. Fang, Y. Q. Xie, N. F. Zheng, *J. Mater. Chem. A* **2018**, 6, 14571.
- [17] S. Meng, X. Zhao, C. Y. Tang, P. Yu, R. Y. Bao, Z. Y. Liu, M. B. Yang, W. Yang, *J. Mater. Chem. A* **2020**, 8, 2701.
- [18] H. X. Liang, Q. H. Liao, N. Chen, Y. Liang, G. Q. Lv, P. P. Zhang, B. Lu, L. T. Qu, *Angew. Chem. Inter. Edit.* **2019**, 58, 19041.
- [19] G. Wang, Y. Fu, A. K. Guo, T. Mei, J. Y. Wang, J. H. Li, X. B. Wang, *Chem. Mater.* **2017**, 29, 5629.
- [20] Xu, W.; Xing, Y.; Liu, J.; Wu, H.; Cui, Y.; Li, D.; Guo, D.; Li, C.; Liu, A.; Bai, H. *ACS Nano* **2019**, 13, 7930.
- [21] Guo, Y.; Zhao, F.; Zhou, X.; Chen, Z.; Yu, G. *Nano Lett.* **2019**, 19, 2530-2536.
- [22] Jiang, Q.; Gholami Derami, H.; Ghim, D.; Cao, S.; Jun, Y.-S.; Singamaneni, S. *J. Mater. Chem. A* **2017**, 5, 18397-18402.
- [23] Zhou, L.; Tan, Y.; Wang, J.; Xu, W.; Yuan, Y.; Cai, W.; Zhu, S.; Zhu, J. *Nature Photon.* **2016**, 10, 393-398.
- [24] Chen, Q.; Pei, Z.; Xu, Y.; Li, Z.; Yang, Y.; Wei, Y.; Ji, Y. *Chem. Sci.* **2018**, 9, 623-628.
- [25] Zhu, M.; Li, Y.; Chen, G.; Jiang, F.; Yang, Z.; Luo, X.; Wang, Y.; Lacey, S. D.; Dai, J.; Wang, C.; Jia, C.; Wan, J.; Yao, Y.; Gong, A.; Yang, B.; Yu, Z.; Das, S.; Hu, L. *Adv. Mater.* **2017**, 29.
- [26] Z. W. Huang, Z. J. Li, L. R. Zheng, L. M. Zhou, Z. F. Chai, X. L. Wang, W. Q. Shi, *Chem. Eng. J.* **2017**, 328, 1066.
- [27] L. L. Chen, S. J. Feng, D. L. Zhao, S. H. Chen, F. F. Li, C. L. Chen, *J. Colloid Interface Sci.* **2017**, 490, 197.
- [28] Y. Li, L. Y. Li, T. Chen, T. Duan, W. T. Yao, K. Zheng, L. C. Dai, W. K. Zhu, *Chem. Eng. J.* **2018**, 347, 407.
- [29] Z. B. Zhang, Z. M. Dong, X. X. Wang, Y. Dai, X. H. Cao, Y. Q. Wang, R. Hua, H. T. Feng, J. R. Chen, Y. H. Liu, B. W. Hu, X. K. Wang, *Chem. Eng. J.* **2019**, 370, 1376.
- [30] Y. W. Cai, X. Wang, J. H. Feng, M. Y. Zhu, A. Alsaedi, T. Hayat, X. L. Tan, *Environ. Pollut.* **2019**, 249, 434.
- [31] X. J. Guo, H. C. Yang, Q. Liu, J. Y. Liu, R. R. Chen, H. S. Zhang, J. Yu, M. L. Zhang, R. M. Li, J. Wang, *Chem. Eng. J.* **2020**, 382.
- [32] Sun, Q.; Aguilera, B.; Earl, L. D.; Abney, C. W.; Wojtas, L.; Thallapally, P. K.; Ma, S. *Adv. Mater.* **2018**, 30, e1705479.
- [33] Aguilera, B.; Sun, Q.; Cassady, H.; Abney, C. W.; Li, B.; Ma, S. *ACS Appl. Mater. Inter.* **2019**, 11, 30919.

- [34] Li, J. Q.; Gong, L. L.; Feng, X. F.; Zhang, L.; Wu, H. Q.; Yan, C. S.; Xiong, Y. Y.; Gao, H. Y.; Luo, F. *Chem. Engineer. J.* **2017**, 316, 154-159.
- [35] Li, B.; Sun, Q.; Zhang, Y.; Abney, C. W.; Aguilera, B.; Lin, W.; Ma, S. *ACS Appl. Mater. Inter.* **2017**, 9, 12511-12517.
- [36] Dai, Z.; Sun, Y.; Zhang, H.; Ding, D.; Li, L. *Journal. Chem. & Engineer. Data* **2019**, 64, 5797-5805.
- [37] Wang, D.; Song, J.; Lin, S.; Wen, J.; Ma, C.; Yuan, Y.; Lei, M.; Wang, X.; Wang, N.; Wu, H. *Adv. Funct.l Mater.* **2019**, 29.
- [38] Wang, T.; Xu, M.; Han, X.; Yang, S.; Hua, D. *J Hazard Mater.* **2019**, 368, 214-220.
- [39] Ma, H.; Zhang, F.; Li, Q.; Chen, G.; Hu, S.; Cheng, H. *RSC Adv.* **2019**, 9, 18406-18414.
- [40] Yuan, Y.; Yu, Q.; Wen, J.; Li, C.; Guo, Z.; Wang, X.; Wang, N. *Angew Chem. Int. Ed.* **2019**, 58, 11785-11790.
- [41] Wang, G.; Liu, J.; Wang, X.; Xie, Z.; Deng, N. *J Hazard Mater.* **2009**, 168, 1053-8.
- [42] Zhang, T.; Ling, B.-K.; Hu, Y.-Q.; Han, T.; Zheng, Y.-Z. *Cryst. Eng. Comm.* **2019**, 21, 3901-3905.
- [43] Yuan, Y.; Feng, S.; Feng, L.; Yu, Q.; Liu, T.; Wang, N. *Angew. Chem. Int. Ed.* **2020**, 59, 4262-4268.
- [44] Yuan, Y.; Yang, Y.; Ma, X.; Meng, Q.; Wang, L.; Zhao, S.; Zhu, G. *Adv. Mater.* **2018**, 30, e1706507.
- [45] Yuan, Y.; Niu, B.; Yu, Q.; Guo, X.; Guo, Z.; Wen, J.; Liu, T.; Zhang, H.; Wang, N. *Angew. Chem. Int. Ed.* **2020**, 59, 1220-1227.
- [46] Yuan, Y.; Zhao, S.; Wen, J.; Wang, D.; Guo, X.; Xu, L.; Wang, X.; Wang, N. *Adv. Funct.l Mater.* **2019**, 29.
- [47] Wang, D.; Song, J.; Wen, J.; Yuan, Y.; Liu, Z.; Lin, S.; Wang, H.; Wang, H.; Zhao, S.; Zhao, X.; Fang, M.; Lei, M.; Li, B.; Wang, N.; Wang, X.; Wu, H. *Adv. Energy Mater.* **2018**, 8.
- [48] Yuan, Y.; Yu, Q.; Wen, J.; Li, C.; Guo, Z.; Wang, X.; Wang, N. *Angew. Chem. Int. Ed.* **2019**, 58, 11785-11790.